

# Constraining the instantaneous aerosol influence on cloud albedo

Edward Gryspeerdt<sup>a,b,1</sup>, Johannes Quaas<sup>a</sup>, Sylvaine Ferrachat<sup>c</sup>, Andrew Gettelman<sup>d</sup>, Steven Ghan<sup>e</sup>, Ulrike Lohmann<sup>c</sup>, Hugh Morrison<sup>d</sup>, David Neubauer<sup>c</sup>, Daniel G. Partridge<sup>f,g</sup>, Philip Stier<sup>h</sup>, Toshihiko Takemura<sup>i</sup>, Hailong Wang<sup>e</sup>, Minghui Wang<sup>j,k,l,e</sup>, and Kai Zhang<sup>e</sup>

<sup>a</sup>Institute for Meteorology, Universität Leipzig, Leipzig, Germany; <sup>b</sup>Space and Atmospheric Physics Group, Imperial College London, London SW7 2AJ, United Kingdom; <sup>c</sup>Institute for Atmospheric and Climate Science, ETH Zurich, 8092 Zurich, Switzerland; <sup>d</sup>National Center for Atmospheric Research, Boulder, CO 80305; <sup>e</sup>Atmospheric Sciences and Global Change Division, Pacific Northwest National Laboratory, Richland, WA 99352; <sup>f</sup>Department of Environmental Science and Analytical Chemistry, Stockholm University, Stockholm, Sweden; <sup>g</sup>Bert Bolin Centre for Climate Research, Stockholm University, Stockholm, Sweden; <sup>h</sup>Atmospheric, Oceanic and Planetary Physics, Department of Physics, University of Oxford, Oxford, OX1 3PU, United Kingdom; <sup>i</sup>Research Institute for Applied Mathematics, Kyushu University, Fukuoka 816-8580, Japan; <sup>j</sup>Institute for Climate and Global Change Research, Nanjing University, 210023 Nanjing, China; <sup>k</sup>School of Atmospheric Sciences, Nanjing University, 210023 Nanjing, China; <sup>l</sup>Collaborative Innovation Center of Climate Change, 210023 Nanjing, China

This manuscript was compiled on May 2, 2017

**Much of the uncertainty in estimates of the anthropogenic forcing of climate change comes from uncertainties in the instantaneous effect of aerosols on cloud albedo, known as the Twomey effect or the radiative forcing from aerosol-cloud interactions (RFaci) a component of the total or effective radiative forcing (ERFaci). As aerosols serving as cloud condensation nuclei (CCN) can have a strong influence on the cloud droplet number concentration ( $N_d$ ), previous studies have used the sensitivity of the  $N_d$  to aerosol properties as a constraint on the strength of the RFaci. However, recent studies have suggested that relationships between aerosol and cloud properties in the present day climate may not be suitable for determining the sensitivity of the  $N_d$  to anthropogenic aerosol perturbations. Using an ensemble of global aerosol-climate models, this study demonstrates how joint histograms between  $N_d$  and aerosol properties can account for many of the issues raised by previous studies. It shows that if the anthropogenic contribution to the aerosol is known, the RFaci can be diagnosed to within 20% of its actual value. The accuracy of different aerosol proxies for diagnosing the RFaci is investigated, confirming that using the aerosol optical depth (AOD) significantly underestimates the strength of the aerosol-cloud interactions in satellite data.**

Aerosols | Clouds | Radiative Forcing

The radiative forcing due to anthropogenic aerosols is the most uncertain component of the anthropogenic radiative forcing [1], with the interaction between aerosols and clouds generating much of this uncertainty. As cloud droplets form on aerosol particles, changes in the aerosol number concentration can change the cloud droplet number concentration ( $N_d$ ), generating an instantaneous radiative forcing by increasing the cloud brightness known as the “Twomey effect” [2] or RFaci [1] (referring only to liquid clouds in this work). Together with other changes in cloud properties due to changes in  $N_d$  [eg. 3], the RFaci is a component of the ERFaci.

Due to the sparse nature of pre-industrial observations of cloud properties, the influence of aerosols on cloud properties is often inferred from observations of the present-day spatio-temporal variability of aerosol and cloud properties [eg. 4–7]. While much of the variation between aerosol and cloud properties can be attributed to variations of meteorological factors [eg. 8, 9], the sensitivity of  $N_d$  to aerosol optical depth (AOD) is thought to be largely independent of these factors. It is therefore often used in observational estimates of the strength of aerosol-cloud interactions [7, 10, 11]. This sensitiv-

ity [5] has been shown to be a useful “emergent constraint” on the strength of the ERFaci in general circulation models [12], providing a method to calculate the change in  $N_d$  from the pre-industrial (PI) to the present day (PD), when combined with an estimate of the corresponding anthropogenic change in AOD (such as [13]). Two main assumptions are made in this process, firstly that the AOD is a suitable proxy of the cloud condensation nuclei (CCN) concentration at the cloud base. Second, that the relationships between aerosol and the  $N_d$  in the present day (determined by spatio-temporal variability) are indicative of the actual sensitivity of cloud properties to aerosol perturbations.

Recent work has called both of these assumptions into question. Observational [14] and model-based [15] studies have shown a disconnect between AOD and CCN. As the AOD is a column integrated measurement, it does not provide vertical information about the location of the aerosol. It also lacks information about the composition of the particles and is weighted preferentially towards larger particles [4], missing information about smaller aerosol particles that are often emitted from anthropogenic activities [16].

Second, it has been shown that the PD AOD- $N_d$  relationship may not be representative of the true strength of the

## Significance Statement

Uncertainties in the strength of aerosol-cloud interactions drive the current uncertainty in the anthropogenic forcing of the climate. Previous studies have highlighted shortcomings in using satellite data for determining the forcing, which underestimate the strength of the aerosol forcing. This work demonstrates that the component of the radiative forcing from aerosol-cloud interactions due to the instantaneous effect on cloud reflectivity (RFaci) can be calculated to within 20%, using only present day observations of the variability of aerosol and cloud properties, provided the anthropogenic component of the aerosol is known. The model results are combined with satellite data to provide an improved observations-based estimate of the RFaci, paving the way for more accurate estimates of the aerosol influence on climate.

EG and JQ wrote the paper, EG performed the analysis, SF, AG, SG, UL, HM, DN, DGR, PS, TT, HW, MW and KZ contributed new reagents/analytic tools.

The authors declare no conflicts of interest.

<sup>1</sup>To whom correspondence should be addressed. E-mail: e.gryspeerdt@imperial.ac.uk

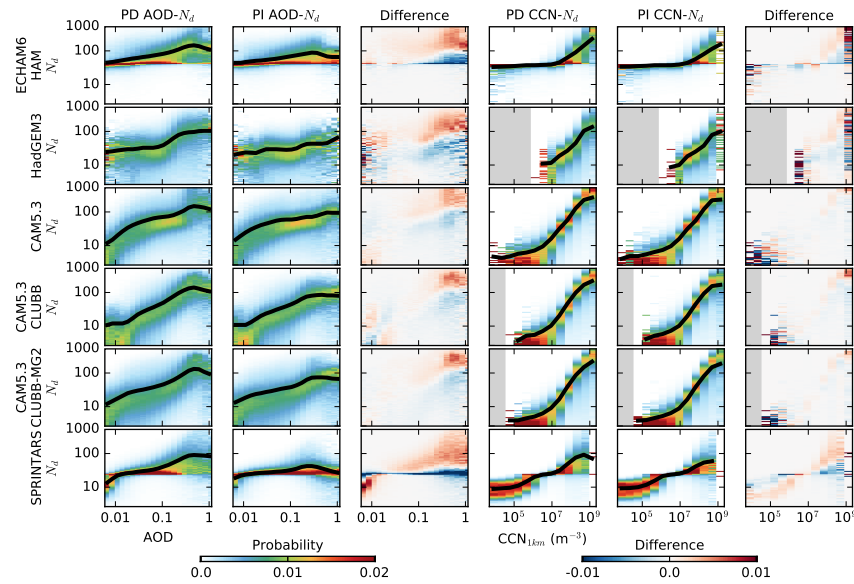


**Fig. 1.** Joint histograms between aerosol properties (AOD and  $CCN_{1km}$ , respectively, x-axis) and cloud top  $N_d$  (y-axis) for each of the GCMs used in this study. The first and second columns show the AOD- $N_d$  joint histograms for the present day and the pre-industrial simulations respectively. The histograms are normalised so each column sums to one, such that the histograms show the probability of observing a specific cloud top  $N_d$ , given a certain AOD (or  $CCN_{1km}$ ). The black line shows the mean  $N_d$  at each AOD and grey regions indicate missing data. The third column shows the difference between the present day and the pre-industrial relationships. The second set of three columns are the same as the first three, but use  $CCN_{1km}$  at 0.3% supersaturation instead of AOD as the independent variable.

interaction between aerosols and cloud properties due to the differing PI and PD aerosol environments [17]. Additionally, it has been shown [18] that in many global aerosol-climate models, the PD sensitivity of  $N_d$  to CCN variations (the slope of the linear regression between  $N_d$  and CCN concentrations) is in many cases not representative of the sensitivity of  $N_d$  to the anthropogenic perturbation of CCN (the PD-PI change in  $N_d$  divided by the corresponding change in CCN evaluated from climate simulations). This suggests that it would be challenging to constrain the magnitude of the RFaci using only PD observations of the sensitivity of  $N_d$  to aerosol variations.

In this work, new techniques are presented to address these challenges. To account for non-linearity in the aerosol- $N_d$  relationship and the differing PI and PD aerosol environments, normalised joint histograms are used to characterise the relationship [following 11]. A variety of different global aerosol-climate models that contributed to the AeroCom intercomparison [18, 19] are used to investigate the utility of different aerosol proxies for diagnosing the anthropogenic change in cloud-top  $N_d$ . Together with joint histograms, this work investigates how accurately the RFaci could be diagnosed under ideal conditions, using present day relationships between aerosol and cloud properties.

## Results

**Aerosol- $N_d$  relationships.** Two-dimensional (“joint”) histograms of  $N_d$  and aerosol properties are used in this work to account for the influence of non-linearities in the relationship [11]. Each column of the joint histogram is normalised so that it sums to one, such that it becomes an array of conditional probabilities. For example, the top left histogram in Fig. 1 shows the probability of finding a specific  $N_d$ , given that a certain AOD has been observed.

Joint histograms of cloud top  $N_d$  versus an aerosol proxy for a selection of models from the AeroCom intercomparison [18, 19] (gridded to  $2.5^\circ$  by  $2.5^\circ$ ) are shown in Fig. 1. While there is a general increase in cloud top  $N_d$  with increasing AOD (Fig. 1, first and second columns), the nature of this increase varies significantly amongst the models. Some of the models (the CAM5 variants) show a strong increase in  $N_d$  at lower AOD, followed by a saturation at higher AOD, where the  $N_d$  only weakly increases with increasing AOD. Others show a weak AOD- $N_d$  relationship at low AOD, followed by a stronger relationship as the AOD increases (ECHAM6-HAM, SPRINTARS). The enforced lower bound to the  $N_d$  apparent in some simulations may be responsible for the lower sensitivity of  $N_d$  to AOD ( $\frac{dN_d}{d\ln(A)}$ ) at low AODs in these models [12], although low sensitivities at low AOD have also been observed in satellite data [11].

All of the models show some difference in the AOD- $N_d$  relationship between the PD and the PI (Fig. 1, third column), mostly with higher  $N_d$ s for a given AOD in the PD simulation compared to the PI. It is stronger at high AODs, suggesting that this effect is due to the different composition of aerosols in the PD compared to the PI. When the atmosphere is clean (low AOD), the aerosol composition is similar in the PI and the PD simulations. However, high AOD conditions occur mainly in dusty regions in the PI simulation (where the aerosol is a poor CCN), but in the PD simulation, these high AOD conditions are often the result of anthropogenic pollution (which on average is a much better CCN).

The situation is very different when using CCN at 1 km altitude and 0.3% supersaturation ( $CCN_{1km}$ ) instead of the AOD as the parameter representing the aerosol (Fig. 1, fourth column). The  $CCN_{1km}$ - $N_d$  relationships are still mostly non-linear, although there is less variation between the models than for the AOD- $N_d$  joint histograms. Importantly, the PD and

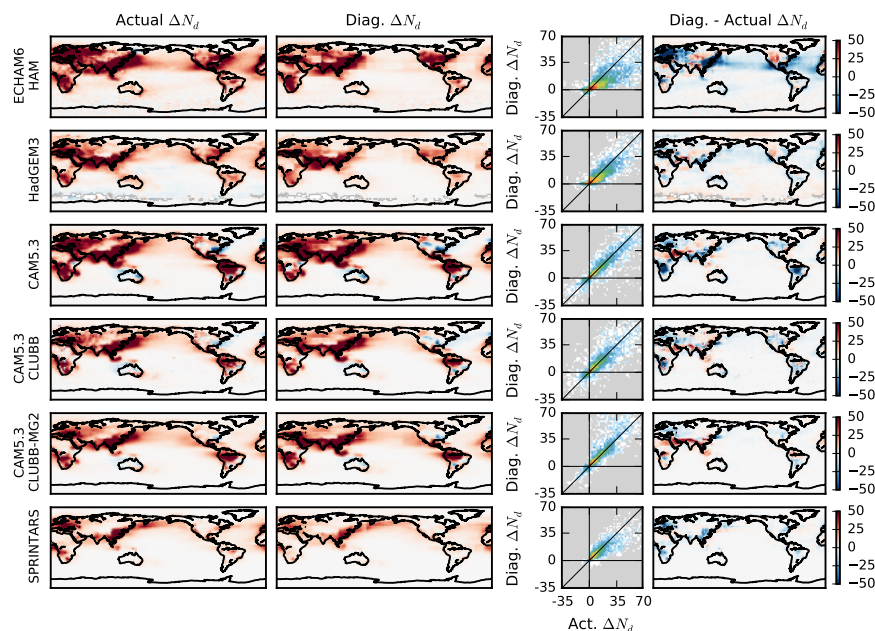


**Fig. 2.** Using joint histograms of  $\text{CCN}_{1\text{km}}$  vs.  $N_d$  from  $15^\circ$  by  $15^\circ$  regions to diagnose  $\Delta N_d$  (Hist CCN regional). For each model used, the first column shows the annual-mean “actual”  $\Delta N_d$  (the  $N_d$  difference between the PI and PD simulations). The second shows  $\Delta N_d$  diagnosed using the present day  $\text{CCN}_{1\text{km}}\text{-}N_d$  joint histogram and the change in the  $\text{CCN}_{1\text{km}}$  between the PI and PD simulations. The third column shows the relationship between the actual and the diagnosed  $\Delta N_d$ , whilst the final column shows the absolute difference between the diagnosed and the actual  $\Delta N_d$ , with red indicating an overestimation in  $\Delta N_d$  diagnosed from the present day relationships compared to the actual value. The same color scale is used for all maps and all the  $N_d$  units are  $\text{cm}^{-3}$ .

PI  $\text{CCN}_{1\text{km}}\text{-}N_d$  relationships are very similar, showing much smaller differences in the joint histograms than are evident for the AOD- $N_d$  relationship (Fig. 1, sixth column). At lower supersaturations (0.1%) the CCN is weighted towards larger particles and the PD and PI relationships are not as close (Fig. S10). However, the PD global  $\text{CCN}_{1\text{km}}\text{-}N_d$  joint histogram is a reasonable indicator of the PI relationship, as long as there is enough data at low CCN concentrations to properly create a joint histogram.

It is also clear that the non-linearity of these relationships will influence any calculations made using a linear regression, where the sensitivity would otherwise depend on the prevailing aerosol environment [17]. By normalising the joint histograms by the aerosol occurrence, this dependence is removed and with the appropriate choice of aerosol proxy (such as  $\text{CCN}_{1\text{km}}$ ), the PD spatio-temporal variability is a good approximation of the PI variation and thus the actual sensitivity of clouds to aerosol perturbations.

**Diagnosing  $\Delta N_d$ .** Using regional joint histograms ( $15^\circ$  by  $15^\circ$  regions), similar to those from Fig. 1, and probability histograms for  $\text{CCN}_{1\text{km}}$  from the PI and PD simulations, a prediction for the geographic distribution of  $\Delta N_d$  is constructed in Fig. 2. The “actual”  $\Delta N_d$  for each model (the difference in  $N_d$  between the PD and PI simulations) is shown in the first column of Fig. 2. Both the PI and PD simulations are nudged to the same horizontal winds, such that the “actual”  $\Delta N_d$  is due to the difference in aerosol emissions. The  $\Delta N_d$  diagnosed using the PD  $\text{CCN}_{1\text{km}}\text{-}N_d$  joint histogram and the PD-PI  $\text{CCN}_{1\text{km}}$  change (Eq. 1) is shown in the second column.

There is a good correspondence between the diagnosed and the actual  $\Delta N_d$  (Fig. 2, third column). The correlation coefficients between the diagnosed and actual  $\Delta N_d$  are between

0.84 and 0.92, explaining between 70% and 85% of the variance (Fig. 3a). These correlations decrease slightly if a single global joint histogram is used (Fig. 3a). The difference between the diagnosed and the actual  $\Delta N_d$  in the fourth column of Fig. 2 varies between the models, partially due to remaining difference between the daily mean  $\text{CCN}_{1\text{km}}$  and the cloud base CCN. This appears to be important for the ECHAM6-HAM simulation over ocean (Fig. 2), where the 1km level is more often above the cloud tops in stratocumulus regions [20] than in the other models. Repeating the analysis using the total column CCN at 0.3% supersaturation (“colCCN”) improves the  $\Delta N_d$  and RFac diagnosis for ECHAM6-HAM (Fig. 3b,c), possibly due to the extra information provided about cloud base CCN. Regime dependent updraughts may also play a role in controlling the remaining 20% of the variability in  $\Delta N_d$  (Fig. 3b). It is possible that there is further variability in  $\Delta N_d$  from PI-PD differences in the parametrised updraughts (which might be reduced by the nudging procedure) but this is a small component of the total variability and so is not further considered in this analysis. These results show that through the ability of the PD  $\text{CCN}_{1\text{km}}\text{-}N_d$  relationship to provide information on the “actual”  $\text{CCN}_{1\text{km}}\text{-}N_d$  relationship, the PD relationship can be used to provide an accurate estimate of the  $\Delta N_d$  due to anthropogenic aerosol perturbations, as long as that perturbation is known.

**Comparison of aerosol proxies.** Although  $\Delta N_d$  can be diagnosed through the PD  $\text{CCN}_{1\text{km}}\text{-}N_d$  relationship, observations of  $\text{CCN}_{1\text{km}}$  are sparse in both space and time, necessitating the use of other aerosol proxies for diagnosing  $\Delta N_d$ . The aerosol index (“AI” - AOD multiplied by Ångström exponent [4]) is routinely observed by satellites and provides more information about aerosol size than the AOD. Although not



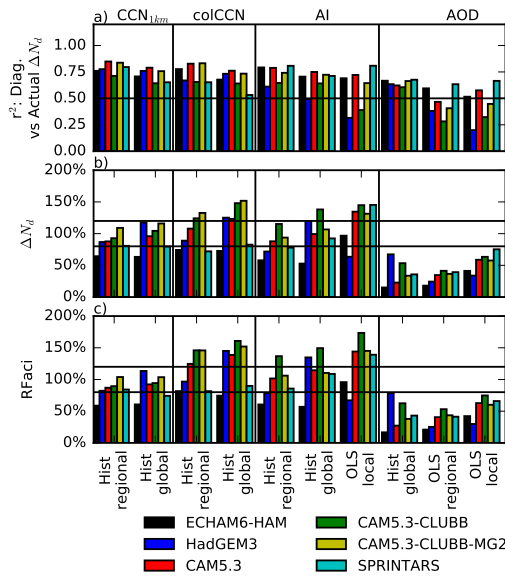


**Fig. 3.** Comparison of different methods and proxies for calculating  $\Delta N_d$ . “Hist” indicates the use of a joint histogram while “OLS” the use of an ordinary least-squares regression. a) Shows the determination coefficient between the diagnosed and the actual values of the  $\Delta N_d$  at a  $2.5^\circ$  by  $2.5^\circ$  resolution globally. b) Shows the relative size of the global mean  $\Delta N_d$  and c) shows the relative size of the implied global mean RFaci, with a percentage less than 100% indicating an underestimate in the estimated RFaci. The horizontal bars are at 80% and 120%. The plots summarised in this figure are shown in Figs. S1-9.

currently retrieved by satellites, colCCN provides extra information about the aerosol chemistry. For each of these proxies, the determination coefficient ( $r^2$ ) between the diagnosed and the actual  $\Delta N_d$  is shown in Fig. 3a (see Figs. S1-9 for other aerosol proxies). For comparison with earlier work, linear regressions between the  $N_d$  and aerosol proxies are also used to characterise the PD aerosol- $N_d$  relationship (“OLS”). The relationships are determined at several different scales:  $2.5^\circ$  by  $2.5^\circ$  degree - “local”;  $15^\circ$  by  $15^\circ$  - “regional” and a single global relationship “global”. The “local” scale is only used with the OLS method, as there is not enough data within each gridbox to generate a full joint histogram.

Using separate regional PD joint histograms between  $CCN_{1km}$  and  $N_d$  (Fig. 3a, Hist regional) is best able to predict  $\Delta N_d$  for each of the models investigated here (excluding ECHAM6-HAM). A single global joint  $CCN_{1km}$ - $N_d$  histogram (Hist global) results in a slight decrease in the ability to predict  $\Delta N_d$ . There is again a slight weakening in predictive ability when moving to the colCCN as a proxy for diagnosing  $\Delta N_d$ . The AI also provides a reasonable parameter for characterising the aerosol, in many cases producing an accurate estimate of  $\Delta N_d$  (Fig. 3b). Using regional AI- $N_d$  joint histograms for diagnosing  $\Delta N_d$  gives  $r^2$  values between the diagnosed and the actual  $\Delta N_d$  (0.61 to 0.81) approaching those of the  $CCN_{1km}$ . As the models do not provide the RFaci, the relative error in the RFaci is estimated by weighting  $\Delta N_d$  by the observed liquid cloud fraction and cloud albedo susceptibility (Fig. 3c, see methods section for details). In general, the regional joint histograms provide a more accurate diagnosis of RFaci, although using a single global histogram results in only a small increase in the error, even though the  $r^2$  value decreases for all

the models (Fig. 3a). The AOD performs worst as a parameter for characterising aerosol in the models when diagnosing  $\Delta N_d$  and RFaci. The local linear regressions have the lowest  $r^2$  values of all the methods and proxies investigated, although the RFaci estimate when using AOD is slightly improved compared to the regional linear regression, possibly due to the reduced aerosol type variability for a local regression (Fig. 3c).

From these results, it is clear that estimates of the aerosol forcing that rely on the relationship between AOD and  $N_d$  for characterising the strength of aerosol cloud interactions (such as many observational estimates) are likely to underestimate the anthropogenic perturbation of  $N_d$  by at least 30% (up to 90%). This would lead to an underestimate in the strength of the radiative forcing from aerosol indirect effects in these studies of at least 20% (up to 90%).

**Satellite based estimate.** Although using the AOD as an aerosol proxy can lead to an underestimate when diagnosing the aerosol forcing, the AI is almost as good a proxy for the aerosol as the  $CCN_{1km}$  when attempting to diagnose  $\Delta N_d$  and the RFaci (Fig. 3c). Given this improved accuracy when compared to using AOD as an aerosol proxy, MODIS AI and  $N_d$  data is used to generate both regional joint histograms (Hist AI regional,  $15^\circ$  by  $15^\circ$  regions) and a single global joint histogram (Hist AI global), using 10 years of data (2004-2013). These are then combined with the annual mean MODIS liquid cloud fraction and the cloud susceptibility derived from MODIS and CERES (Eq. 3) to provide an updated estimate of the RFaci (Fig. 4).

Using the PI to PD AI changes from each of the models gives a range of RFaci estimates for the regional method between  $-0.18$  and  $-0.58 \text{ Wm}^{-2}$  and between  $-0.29$  and  $-1.01 \text{ Wm}^{-2}$  if using a single global AI- $N_d$  joint histogram (Fig. S11). The RFaci is generally higher over the ocean due to the higher liquid cloud fraction and cloud susceptibility, despite the smaller oceanic  $\Delta N_d$  (Fig. 2). Although this is not a large selection of models, the mean value of  $-0.29 \text{ Wm}^{-2}$  for the regional method and  $-0.49 \text{ Wm}^{-2}$  for the global histogram are instructive to compare to the  $-0.2 \text{ Wm}^{-2}$  mean value using a single global AOD- $N_d$  histogram (Fig. 4c),  $-0.2 \text{ Wm}^{-2}$  using local OLS with AOD [7] and  $-0.4 \text{ Wm}^{-2}$  using local OLS and AI [21].

There are some caveats to this estimate. First, the MODIS AI has little quantitative skill over land [22] and in some regions a positive RFaci is diagnosed from changes in the  $N_d$  (Fig. 4). This has a larger impact on the regional histogram method and may result in a reduction in the strength of the implied aerosol forcing. However, only a small fraction of the forcing comes from continental regions, similar to the findings from [7], so this may not result in a large bias in the global mean RFaci. Also, the global histogram method is more likely to overestimate the RFaci (Fig. 3c), suggesting that the actual value is between the two estimates, perhaps around  $-0.4 \text{ Wm}^{-2}$  (this only includes changes to cloud albedo and not other rapid cloud adjustments). It is also possible that systematic biases in the MODIS AI or  $N_d$  retrieval could further impact this result, although the magnitude and sign of these effects is unclear. It should also be noted that this estimate is strongly dependent on the estimate of the anthropogenic aerosol fraction. As all the AeroCom models in this work use the same emissions database, the diversity in the forcing estimates from the models is unlikely to fully represent the full uncertainty in the radiative forcing from changes in cloud albedo.

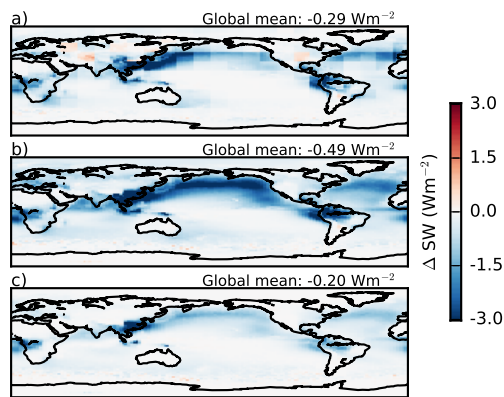


**Fig. 4.** The mean of the individual model RFaci estimates (Fig. S11), using MODIS data to create a) Regional histograms, b) a single global AI- $N_d$  histogram and c) a single global AOD- $N_d$  histogram, combined with model estimates of the anthropogenic AI/AOD contribution.

## Discussion

Previous work has shown that the present day CCN- $N_d$  relationship sampled from spatio-temporal variability is not necessarily representative of the “actual” sensitivity of  $N_d$  to aerosol changes since pre-industrial times. This is partially due to the large errors in the sensitivity of the  $N_d$  to CCN in clean regions, where there is little CCN variation and consequently little  $N_d$  variation in the PD climate. However, these regions are usually regions with a small anthropogenic CCN contribution and so make only a small contribution to the global  $\Delta N_d$ . Although the nudging process might reduce the variability in  $\Delta N_d$  from variations in the in-cloud updraughts, this work demonstrates that the CCN<sub>1km</sub>- $N_d$  relationship is representative enough in regions where there is a large  $\Delta N_d$  to make an accurate prediction of the global  $\Delta N_d$  and RFaci.

It is also interesting to note that the big increases in  $N_d$  occur in regions with large changes in CCN (over land, the northern hemisphere) in all the models investigated here (Fig. 2). While these models implement aerosol activation parametrisations that result in a saturation of the  $N_d$  at high CCN concentrations, this behaviour is not evident in many of the joint histograms of Fig. 1 for the CCN<sub>1km</sub> versus the  $N_d$ . Although there are other non-linearities in the pathway between CCN changes and a change in top of atmosphere albedo [eg. 11], strong aerosol-cloud interaction effects also occur in regions of stronger aerosol perturbation for the CMIP5 models (albeit less concentrated in the northern hemisphere) [23], supporting the idea that the RFaci in remote regions such as the southern ocean does not dominate the total RFaci.

Finally, the results of this work demonstrate the importance of including aerosol size information when making estimates of the aerosol impact on cloud properties. Previous work has shown that the AI correlates better than the AOD with the cloud base CCN [15]. This work shows that it also offers significant benefits as an aerosol proxy when calculating  $\Delta N_d$  and the radiative forcing from aerosol-cloud interactions. The large increase in predictive ability of  $\Delta N_d$  when moving from AOD to AI for characterising the aerosol shows the importance of a measure of aerosol size, especially given the strong changes in aerosol type between the PI and the PD simulations. While

there is also a clear benefit from including vertical information (CCN<sub>1km</sub> is a better proxy than colCCN for most GCMs), this increase in the accuracy when diagnosing the radiative forcing is smaller than that when using AI compared to AOD. The change in predictive ability when moving from AI to column integrated CCN is the smallest change, suggesting that information on aerosol composition is the least important of the three factors (vertical location, size distribution and composition) that limit the ability of the AOD- $N_d$  relationship to characterise the strength of aerosol-cloud interactions [24].

## Conclusions

In this work, multiple aerosol-climate models have been used to investigate how a change in cloud droplet number concentration ( $N_d$ ) can be predicted from present day aerosol-cloud relationships.

The use of joint histograms normalised by aerosol occurrence is demonstrated, accounting for non-linearities in the aerosol- $N_d$  relationship. It also removes the influence of the aerosol environment on the strength of the aerosol- $N_d$  relationship, such that the present day and pre-industrial aerosol- $N_d$  relationships are nearly identical with the correct choice of aerosol proxy (Fig. 1).

Although diagnosing the true sensitivity of  $N_d$  to cloud condensation nuclei (CCN) remains a difficult problem using only present day relationships [18], determining  $\Delta N_d$  is much easier as it weights the calculation towards regions with a larger change in CCN, where the relationship can be determined with greater accuracy in (Fig. 2). If the change in CCN at 1km altitude (CCN<sub>1km</sub>) between the pre-industrial (PI) and the present day (PD) is known, then the PD relationship between CCN<sub>1km</sub> and the  $N_d$  is enough to diagnose the PD-PI change in  $N_d$  ( $\Delta N_d$ ) to within 20% of the value determined by the climate simulations (Fig. 3). Using joint histograms to account for non-linearities in the CCN- $N_d$  relationship, a single global relationship between CCN<sub>1km</sub> and  $N_d$  can be used, with only a small reduction in the accuracy of diagnosing  $\Delta N_d$  and the instantaneous radiative forcing due to changes in cloud albedo (RFaci).

While vertical information is shown to be important in predicting  $\Delta N_d$ , these results imply that information about the aerosol size distribution makes a dominant contribution to the accuracy of the predictions of  $\Delta N_d$ , with the aerosol index (AI) showing significant gains over the aerosol optical depth (AOD), similar to previous work [15]. The estimates of the anthropogenic change in AI provided by the models in this work combined with AI- $N_d$  joint histograms from satellite data provide a revised RFaci estimate of around  $-0.4 \text{ Wm}^{-2}$ , although there is a large diversity between the model estimates, ranging from  $-0.18$  to  $-1.01 \text{ Wm}^{-2}$ . The larger  $\Delta N_d$  suggested by this work also suggests a larger ERFaci than previous studies [11], but this not investigated here. As estimates of the PD-PI aerosol environment are often generated from models, estimates of the PD-PI AI change could be calculated alongside AOD changes. Using AI has the advantage over using CCN since it is currently retrieved by satellite instruments (although retrieving CCN may be possible in certain situations [25]). This suggests that the AI is potentially a useful parameter to use when calculating observational constraints on the strength of RFaci in liquid clouds and where possible should be considered for future observation-based investigations.

## Materials and Methods

Throughout this work, output from several global aerosol-climate simulations performed as part of the AeroCom model inter-comparison project [18, 19] is used to provide simulations of the PD and PI atmospheres. Both PD and PI simulations are nudged to the same horizontal winds (2006–2010) and include PD greenhouse gases, sea surface temperatures and natural forcings. All of the models include interactive aerosol modules, that interact with the cloud via a modification of  $N_d$ , ice crystal number concentration and radiative fluxes. This affects the radiation as well as the precipitation formation in liquid clouds via autoconversion, leading to more complex effects on the cloud properties. The model data is regridded to a  $2.5^\circ$  by  $2.5^\circ$  resolution and averaged to daily temporal resolution. As this analysis focuses on liquid water clouds, only gridboxes with an ice water path of less than  $5 \text{ g m}^{-2}$  are used. Six of the nine available simulations were selected to provide a wide selection of models and microphysics schemes. The models themselves are self-consistent, such that an imperfect modelling of the aerosol or the cloud properties does not affect the conclusions.

$\Delta N_d$  is diagnosed for each  $2.5^\circ$  by  $2.5^\circ$  gridbox using the PD relationship between the aerosol parameter ( $A$ ) and the  $N_d$  and the known change in the aerosol parameter between the PD and PI simulations. Eq. 1 shows how  $\Delta N_d$  is diagnosed within each gridbox using a joint probability histogram between the aerosol and  $N_d$  created from PD relationships and the probability histograms of the PI and PD aerosol parameter in each gridbox.

$$\Delta N_d = \sum_{N_d} N_d \sum_A P(N_d|A)_{PD} \times (P(A)_{PD} - P(A)_{PI}) \quad [1]$$

If the OLS method is used, the calculation for  $\Delta N_d$  is conceptually similar, using the ACI metric ( $\frac{dN_d}{d\ln(A)}_{PD}$ ) from [5].

$$\Delta N_d = ACIA \times \left( \overline{\ln(A_{PD})} - \overline{\ln(A_{PI})} \right) \quad [2]$$

where the overbar denotes an average over a distribution. To investigate the impact that errors in diagnosing  $\Delta N_d$  have on the RFaci, the Twomey formula [26] is used to calculate the change in cloud albedo ( $\alpha_{cld}$ ). The cloud albedo is calculated from the CERES TOA SW all-sky albedo and the MODIS Aqua L3 (MYD08\_D3) collection 6 cloud optical properties cloud fraction [27], using only gridboxes with zero ice cloud. This is combined with the MODIS annual mean liquid cloud fraction ( $f_{liq}$ ) and the downwelling solar flux ( $F^\downarrow$ ) to produce a simple estimate of the RFaci ( $\Delta F^\uparrow$ ) [28].

$$\Delta F^\uparrow = -F^\downarrow f_{liq} \frac{\alpha_{cld}(1 - \alpha_{cld})}{3N_d} \Delta N_d \quad [3]$$

The MODIS AI is used to provide an observational constraint on the RFaci by generating AI- $N_d$  joint histograms from observations. For these histograms, the  $N_d$  is calculated using the adiabatic approximation, as specified in [11]. The AI is calculated from the AOD-Angström exponent joint histogram in the MODIS MYD08\_D3 product using only gridboxes where no ice cloud is detected (to reduce possible cirrus contamination). As the relative error of the MODIS AOD and hence the Angström exponent and AI is large at low AOD ( $<0.03$ ), the  $N_d$  is assumed constant at AI values below 0.03.

**ACKNOWLEDGMENTS.** The model data was provided through the AeroCom initiative. The MODIS data was provided by the NASA Goddard Space Flight Center and the CERES data from the NASA Langley Research Center. This work received funding from the European Research Council under the European Union's Seventh Framework Programme (FP7/2007-2013) / ERC grant agreements no. FP7-306284 ("QUAERERE"), FP7-280025 ("ACCLAIM") and FP7-603445 ("BACCHUS"), the United Kingdom Natural Environment Research Council Grant NE/I020148/1, the Austrian Science Fund (J 3402-N29, Erwin Schrödinger Fellowship Abroad), the Environment Research and Technology Development Fund (S-12-3) of the Ministry of the Environment, Japan and JSPS KAKENHI Grant Number JP15H01728 and JP15K12190, the National Natural Science Foundation of China (grant no. 41575073 and 41621005), the Swiss National Supercomputing Centre (project s431) and the supercomputer system of the National Institute for Environmental Studies, Japan. The Pacific Northwest National Laboratory (PNNL) is operated for the Department of Energy (DOE) by Battelle Memorial Institute under Contract DE-AC06-76RLO 1830. Work at PNNL was supported by the US DOE Decadal and Regional Climate Prediction using Earth System Models program and by the US DOE Earth System Modeling program. The ECHAM6-HAM model was developed by a consortium composed of ETH Zurich, Max Planck Institut für Meteorologie, Forschungszentrum Jülich, University of Oxford, the Finnish Meteorological Institute, and the Leibniz Institute for Tropospheric Research, and is managed by the Center for Climate Systems Modeling (C2SM) at ETH Zurich which also provided technical and scientific support. The authors would like to thank Helen Brindley (Imperial College London) for her comments on the manuscript.

- Boucher O et al. (2013) *Clouds and Aerosols*, eds. Stocker T et al. (Cambridge University Press, Cambridge, United Kingdom and New York, NY, USA), p. 571–658.
- Twomey S (1974) Pollution and the planetary albedo. *Atm. Env.* 8:1251–1256.
- Albrecht B (1989) Aerosols, cloud microphysics, and fractional cloudiness. *Science* 245:1227–1230.
- Nakajima T, Higurashi A, Kawamoto K, Penner J (2001) A possible correlation between satellite-derived cloud and aerosol microphysical parameters. *Geophys. Res. Lett.* 28:1171–1174.
- Feingold G, Eberhard W, Veron D, M P (2003) First measurements of the Twomey indirect effect using ground-based remote sensors. *Geophys. Res. Lett.* 30:1287.
- Koren I, Kaufman Y, Rosenfeld D, Remer L, Rudich Y (2005) Aerosol invigoration and restructuring of Atlantic convective clouds. *Geophys. Res. Lett.* 32:L14828.
- Quaas J, Boucher O, Bellouin N, Kinne S (2008) Satellite-based estimate of the direct and indirect aerosol climate forcing. *J. Geophys. Res.* 113:D05204.
- Quaas J, Stevens B, Stier P, Lohmann U (2010) Interpreting the cloud cover - aerosol optical depth relationship found in satellite data using a general circulation model. *Atmos. Chem. Phys.* 10:6129–6135.
- Grandey BS, Gururaj A, Stier P, Wagner TM (2014) Rainfall-aerosol relationships explained by wet scavenging and humidity. *Geophys. Res. Lett.* 41:5678–5684.
- Jones TA, Christopher SA, Quaas J (2009) A six year satellite-based assessment of the regional variations in aerosol indirect effects. *Atmos. Chem. Phys.* 9:4091–4114.
- Gryspeerdt E, Quaas J, Bellouin N (2016) Constraining the aerosol influence on cloud fraction. *J. Geophys. Res.* 121(7):3566–3583.
- Quaas J et al. (2009) Aerosol indirect effects - general circulation model intercomparison and evaluation with satellite data. *Atmos. Chem. Phys.* 9:8697–8717.
- Bellouin N et al. (2013) Impact of the modal aerosol scheme GLOMAP-mode on aerosol forcing in the Hadley Centre global environmental model. *Atmos. Chem. Phys.* 13:3027–3044.
- Shinozuka Y et al. (2015) The relationship between cloud condensation nuclei (CCN) concentration and light extinction of dried particles: indications of underlying aerosol processes and implications for satellite-based CCN estimates. *Atmos. Chem. Phys.* 15:7585–7604.
- Stier P (2016) Limitations of passive remote sensing to constrain global cloud condensation nuclei. *Atmos. Chem. Phys.* 16(10):6595–6607.
- Kaufman YJ et al. (2005) Aerosol anthropogenic component estimated from satellite data. *Geophys. Res. Lett.* 32:L17804.
- Penner JE, Xu L, Wang M (2011) Satellite methods underestimate indirect climate forcing by aerosols. *Proc. Natl. Acad. Sci. USA* 108:13404.
- Ghan S et al. (2016) Challenges in constraining anthropogenic aerosol effects on cloud radiative forcing using present-day spatiotemporal variability. *Proc. Nat. Acad. Sci.* 113:5804–5811.
- Zhang S et al. (2016) On the characteristics of aerosol indirect effect based on dynamic regimes in global climate models. *Atmos. Chem. Phys.* 16(5):2765–2783.
- Nam C, Bony S, Dufresne JL, Chepfer H (2012) The 'too few, too bright' tropical low-cloud problem in CMIP5 models. *Geophys. Res. Lett.* 39(21):L21801.
- Lebsock M, Stephens G, Kummerow C (2008) Multisensor satellite observations of aerosol effects on warm clouds. *J. Geophys. Res.* 113:D15205.
- Levy R et al. (2010) Global evaluation of the collection 5 MODIS dark-target aerosol products over land. *Atmos. Chem. Phys.* 10:10399–10420.
- Zelinka MD, Andrews T, Forster PM, Taylor KE (2014) Quantifying components of aerosol-cloud-radiation interactions in climate models. *J. Geophys. Res.* 119:7599–7615.
- Dusek U et al. (2006) Size matters more than chemistry for cloud-nucleating ability of aerosol particles. *Science* 312:1375–1378.
- Rosenfeld D et al. (2016) Satellite retrieval of cloud condensation nuclei concentrations by using clouds as ccn chambers. *Proc. Nat. Acad. Sci.* 113(21):5828–34.
- Twomey S (1991) Aerosols, clouds and radiation. *Atm. Env* 25:2435–2442.
- Platnick S et al. (2003) The MODIS cloud products: algorithms and examples from Terra. *IEEE T. GeoSci. Remote* 41:459.
- Charlson RJ et al. (1992) Climate forcing by anthropogenic aerosols. *Science* 255:423–430.